Ab initio spin-orbit CI calculations of the potential curves and radiative lifetimes of low-lying states of lead monofluoride

Kalyan K. Das,[a)] Ioannis D. Petsalakis,[b)] Heinz-Peter Liebermann, Aleksey B. Alekseyev, and Robert J. Buenker
FB 9—Theoretische Chemie, Bergische Universität Wuppertal, Gaussstrasse 20, D-42097 Wuppertal, Germany

The electronic structure of the lead monofluoride molecule is studied by means of *ab initio* configuration interaction (CI) calculations including the spin-orbit interaction. Potential-energy curves are generated for a large number of electronic states, of which only the $X_1\,^2\Pi_{1/2}$ ground and $X_2\,^2\Pi_{3/2}$ and $A\,^2\Sigma^+$ excited states have been observed experimentally. Two different methods are compared for the inclusion of spin-orbit effects in the theoretical treatment, a contracted CI which employs a basis of large-scale $\Lambda-S$ eigenfunctions to form a rather small matrix representation of the full relativistic Hamiltonian (two-step approach), and a more computationally laborious technique which involves solution of a secular equation of order $250\,000\,S^2$ eigenfunctions of different spin and spatial symmetry to achieve a potentially more evenly balanced description of both relativistic and electron correlation effects (one-step approach). In the present application, it is found that both methods achieve quite good agreement with measured spectroscopic constants for the X_1, X_2, and A states. The simpler of these methods is also employed to predict the radiative lifetimes of the latter two states. The key $A\,^2\Sigma^+-X\,^2\Pi$ transition moment in these calculations is found to vary strongly with internuclear distance and to vanish in the neighborhood of the respective equilibrium distances of both participating states. The computed lifetime for the A, $v'=0$ state of 16 μs overestimates the corresponding measured value by a factor of three, but those of higher vibrational states are found to decrease rather sharply with increasing v', suggesting that only a slight displacement of the theoretical $A-X$ transition moment curve is needed to explain the above discrepancy. © *2002 American Institute of Physics.* [DOI: 10.1063/1.1423944]

I. INTRODUCTION

The diatomic lead halides PbX have a simple low-energy electronic spectrum, consisting of two bound $\Lambda-S$ states, the spin-orbit split $X\,^2\Pi$ ground state and the $A\,^2\Sigma^+$ first excited state. Both converge to the same asymptotic limit: Pb(^3P) $+X(^2P^o)$. They have recently been observed[1] in the visible and near-infrared region of the spectrum by allowing the corresponding lead dihalide vapors diluted in Ar carrier gas to undergo photolysis by radiation from rare-gas fluoride excimer lasers in a flow system. In particular, it was possible to carry out time-resolved measurements for all four molecules in this series to obtain radiative lifetimes for the first two Ω excited states, $X_2\,^2\Pi_{3/2}$ and $A\,^2\Sigma^+_{1/2}$, both of which emit primarily to the $X_1\,^2\Pi_{1/2}$ ground state. It was found that the A state's lifetime decreases steadily with atomic number of the halogen atom, varying from 5.0±0.8 μs for PbF to 0.13 ±0.03 μs for PbI.[1] On the other hand, the opposite trend is observed for the $X_2\,^2\Pi_{3/2}$ state: 0.36±0.05 ms for PbF and 4.0±0.6 ms for PbI.[1] No explanation for these trends has yet been given, but it seems clear that it can best be sought by carrying out accurate calculations of the corresponding dipole transition moments for these systems.

Over the past eight years, our research group has reported numerous calculations of radiative lifetimes for electronic and vibrational states of diatomic and triatomic molecules containing at least one heavy atom, beginning with a series of Group 15 halides,[2–5] hydrides[6–8] and oxides,[9–11] and more recently with various tellurium compounds,[12–13] BiNa[14] and TlH.[15] In each case direct comparisons between these theoretical and measured lifetimes by the group of Fink, Shestakov, and Setzer at the University of Wuppertal were possible and generally good agreement has been found between these two sets of results. In the present study attention will be centered on the lead monofluoride molecule. The calculations are carried out with the aid of relativistic effective core potentials (RECPs), including spin-orbit coupling, similarly as in the previous examples cited above. A self-consistent field (SCF) treatment is combined with a large-scale configuration interaction (CI) treatment to obtain highly correlated wave functions for PbF at the $\Lambda-S$ level (in the absence of spin-orbit coupling but with inclusion of other scalar relativistic effects). This is followed by a contracted spin-orbit CI (LSC–SO–CI) calculation in which a relatively small secular equation is solved to mix the $\Lambda-S$ states to obtain the final Ω states. Parallel thereto, however, a more computationally demanding approach is applied which

---

a)Permanent address: Department of Chemistry, Physical Chemistry Section, Jadavpur University, Calcutta 700032, India.
b)Permanent address: Theoretical and Physical Chemistry Institute, The Hellenic Research Foundation, 48 Vassileos Constantinou Avenue, 11635 Athens, Greece.

TABLE I. Details of the MRD-CI calculations carried out for various states of the PbF molecule ($r = 3.95\, a_0$, selection threshold $T = 0.5\, \mu E_h$).

C_{2v} symmetry	Number of reference configurations	Number of generated SAFs	Number of selected SAFs	Number of roots	Σc_p^2
$^2A_1$	92	981 813	35 810	9	95.8
$^2A_2$	82	1 175 316	41 096	8	95.4
$^2B_1$, $^2B_2$	134	1 390 421	40 969	9	96.3
$^4A_1$	78	1 085 514	24 760	3	96.3
$^4A_2$	76	1 119 108	26 460	4	96.1
$^4B_1$, $^4B_2$	81	1 053 566	24 348	3	96.5

was first employed in our research group to describe the electronic spectrum of BiH[6] and has since been extended to deal with configuration spaces spanning up to $2 \times 10^6\, S^2$ eigenfunctions.[16,17] In this case the electrostatic and spin-orbit interactions are treated on an equal footing (one-step CI as opposed to the two-step LSC–SO–CI treatment first discussed). In essence, a large secular equation is solved in which configurations from several different spin and spatial symmetries are allowed to interact directly without first obtaining Λ–S wave functions in a treatment which excludes spin-orbit coupling. For relatively light atoms the two procedures should provide similar accuracy, as has been verified in a number of cases in which explicit comparisons have been made.[17] The lead atom ($Z = 82$) is sufficiently heavy that one can expect some significant differences in the results obtained from these two approaches, however, whereby it would seem likely that the more computationally expensive approach would be superior. This aspect of the theoretical calculations has been tested in the present work for the PbF system, albeit only for the total energies of the various electronic states treated.

II. DETAILS OF THE THEORETICAL TREATMENT

The present calculations have been carried out employing an RECP of Christiansen *et al.*[18] which leaves the $5d$, $6s$, and $6p$ shells of lead outside the core to be treated explicitly in the SCF and CI optimizations. The original Cartesian Gaussian atomic orbital (AO) basis recommended in that study has also been used. It consists of five s and five p primitive functions taken in uncontracted form and a single six-component contracted d function. The fluorine $1s$ shell is also represented by a core potential[19] and the original four s and four p primitive basis is employed in uncontracted form. In addition, d and f polarization functions have been included with exponents of 0.7 and $1.5\, a_0^{-2}$, respectively. The first step in the theoretical treatment was to carry out an SCF calculation for the $^2\Sigma^+$ excited state of the PbF molecule, which has a $\pi^4\sigma^*$ electronic configuration. Since the subsequent multireference single- and double-excitation configuration interaction (MRD-CI) treatment is carried out in formal C_{2v} (Abelian) symmetry, an SCF calculation for the $X\,^2\Pi$ ground state has the disadvantage of leading to inequivalent π_x and π_y components, whereby this undesirable feature is not present for a state of Σ symmetry. Some test calculations were also carried out with the $^1\Sigma^+$ SCF MOs of the PbF$^+$ ion, and the results were found to be in excellent agreement with those obtained with the PbF $^2\Sigma^+$ state MO

basis for the same electronic states, as will be discussed in the following section. The F $2s$ and Pb $5d$ SCF orbitals were kept doubly occupied in all configurations, reducing the number of active electrons to nine in the present treatment. A standard perturbative selection procedure[20,21] was used to obtain an appropriate CI space in each case. Separate Λ–S calculations have been carried out for a large series of internuclear distances r for both doublet and quartet states of each C_{2v} irreducible representation. The selection was made at a threshold of $T = 0.5\, \mu E_h$ for a single- and double-excitation space generated from a series of reference configurations chosen on the basis of their contributions to the lowest electronic states of PbF based on the results of preliminary CI calculations. The numbers of reference configurations and roots employed for each Λ–S symmetry are given in Table I, along with typical numbers of selected and generated symmetry-adapted functions (SAFs) for each C_{2v} representation.

The Table-CI algorithm[22–24] is used to evaluate Hamiltonian matrix elements between SAFs and a Direct-CI version of the MRD-CI programs[25–26] has been employed to obtain the resulting energy eigenvalues and eigenfunctions. The sum over squared CI coefficients Σc_p^2 for each of the lowest roots obtained is also given in Table I, and this quantity is generally found to lie in the 95–96% range. The orders of secular equations solved explicitly in the present treatment vary from 25 000 to 40 000, out of a total of $(1.0–1.4) \times 10^6$ SAFs generated by single and double substitutions relative to the reference configurations. An energy extrapolation procedure[20–21] is used to obtain accurate estimates of the CI eigenvalues at zero threshold ($T = 0$) and the multireference analogue of the Davidson correction[27–28] is applied to account for the effects of triple and higher excitations (referred to as the full-CI or FCI correction). In the simpler of the two spin-orbit CI treatments considered, the resulting Λ–S wave functions are used as basis for the matrix representation of the full relativistic Hamiltonian from which the final Ω-state wave functions are obtained by subsequent diagonalization. The M_s components of each doublet and quartet Λ–S state are divided into two degenerate subsets (E_1 and E_2) which form the basis for separate secular equations of order 61 each from which identical LSC–SO–CI eigenvalues ensue (two-step procedure). In the other, more flexible, treatment a Direct SO–CI calculation is carried out for all the SAFs selected for the various Λ–S spaces at $T = 1.0\, \mu E_h$. Near the PbF $X\,^2\Pi$ equilibrium distance ($r = 3.95\, a_0$) the resulting secular equation is of order 250 677,

from which the lowest nine roots have been extracted, similarly as at all other distances treated.

The final phase of the present theoretical treatment is to compute transition and dipole moments between all pairs of $\Lambda - S$ states (with $S_1 = S_2$ and $M_{S_1} = M_{S_2}$) considered above in the LSC–SO–CI two-step approach. The selected-space CI wave functions are used for this purpose, similarly as for the spin-orbit matrix elements mentioned first. The resulting μ_x, μ_y, and μ_z matrices are transformed over the Ω-state SO eigenfunctions, whereby only dipole moment matrix elements for pairs of functions with the same S, M_S values are retained.

All the above calculations have been carried out for a series of r values ranging from 3.2 to $12.0 \, a_0$, in steps of $0.1 \, a_0$ up to $r = 7.5 \, a_0$, and of $0.5 \, a_0$, thereafter up to $r = 10.0 \, a_0$. Additional calculations have been carried out near the ground state's potential minimum (3.85 and $3.95 \, a_0$) and also at $r = 11.0$ and $12.0 \, a_0$. The resulting potential curves are then fit to polynomials which are then used in one-dimensional nuclear motion Schroedinger equations which are solved numerically[29–30] to obtain vibrational energies and eigenfunctions for each electronic state. The dipole moment data are then combined in numerical form with the latter functions to obtain transition moments between pairs of vibrational states, which in turn are used to compute Einstein spontaneous emission coefficients in each case. The latter values for a given upper state are summed over all lower-lying vibrational states to obtain the reciprocal of the latter's radiative lifetime.

III. POTENTIAL ENERGY RESULTS

The computed MRD-CI potential curves for the low-lying states of the PbF molecule obtained without the inclusion of spin-orbit coupling are shown in Fig. 1. The main states of interest in the present study are the $X \, ^2\Pi$ ground state and the $A \, ^2\Sigma^+$ excited state. Their electronic configurations are $\pi^4 \pi^*$ and $\pi^4 \sigma^*$, respectively, near their equilibrium r values. Both states are basically ion-pair in nature (Pb^+F^-) but they dissociate to the same neutral atomic limit, $Pb(^3P) + F(^2P^o)$. As a result both of these potential curves undergo an abrupt change in slope in the $r = 7.0–8.0 \, a_0$ range (Fig. 1). The π^* MO is strongly localized on the lead atom and is therefore nonbonding, whereas the σ^* is much more antibonding and its charge distribution extends over a fairly wide range of r, and its charge center is located $0.27 \, a_0$ farther away from the fluorine atom than is π^*. Almost all other low-lying electronic states have repulsive potentials. The next lowest-energy state is the $a \, ^4\Sigma^-$ with a $\sigma \pi^4 \pi^{*2}$ configuration, and it is a slight exception to the above rule (see Fig. 1). The $2 \, ^2\Sigma^+$ state of the same electronic configuration has a deeper potential minimum than $a \, ^4\Sigma^-$, but its potential curve is crossed by a number of others not far from this minimum and thus is presumably strongly predissociated.

The corresponding Ω-state potential energy curves obtained after inclusion of spin-orbit coupling in the theoretical treatment are shown in Figs. 2(a) and 2(b). The two sets of potentials for the lowest three states are quite similar to one
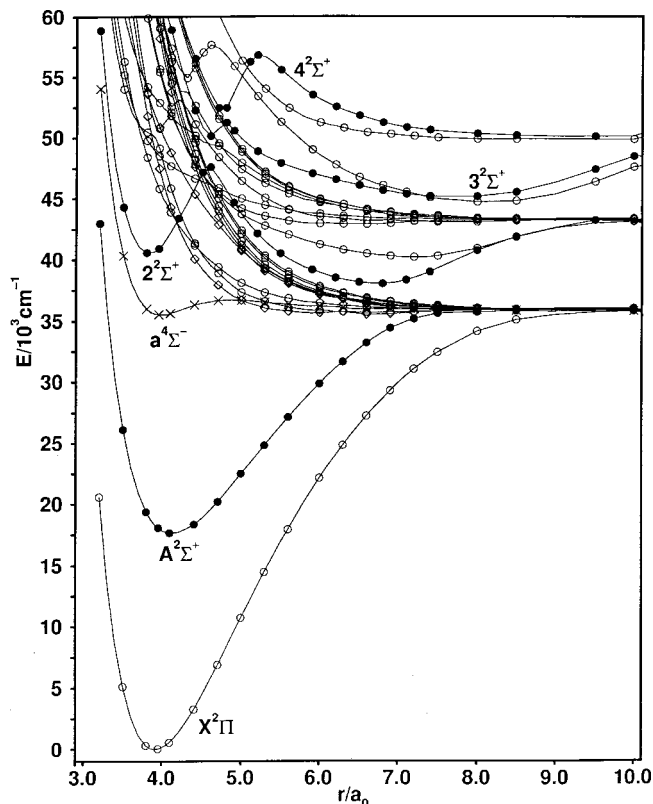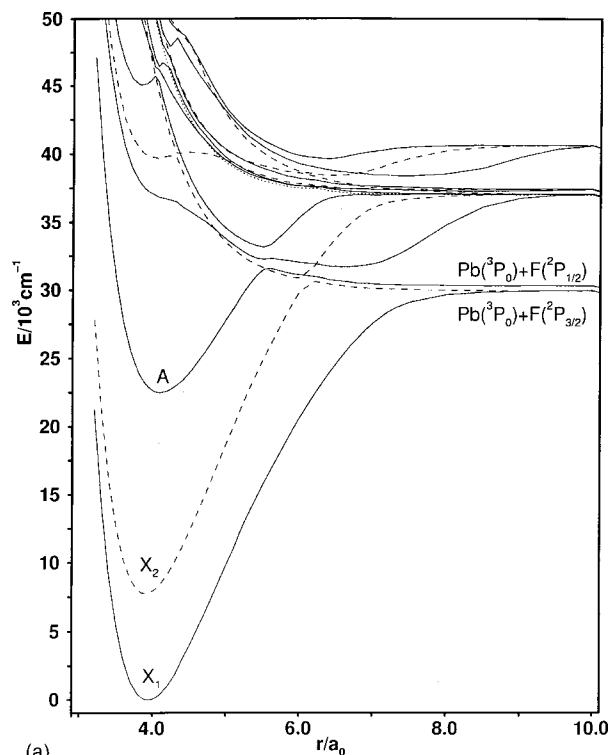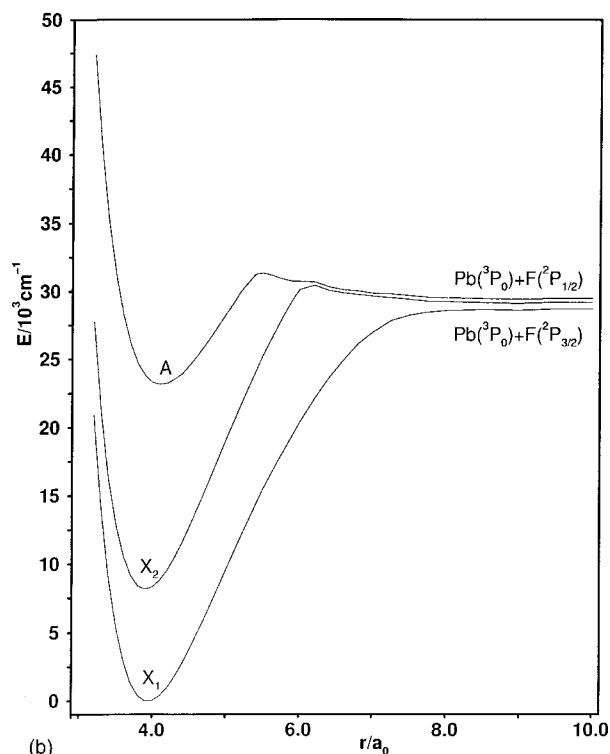

FIG. 1. Computed MRD-CI potential-energy curves for various PbF electronic states obtained without spin-orbit coupling.

another in the two SO-CI approaches [two-step LSC–SO–CI in Fig. 2(a) and the one-step Direct SO–CI in Fig. 2(b)]. The ten lowest-energy eigenvalues for the PbF Ω states have been obtained with both the neutral molecule's $^2\Sigma^+$ SCF MO's and the PbF$^+$ $^1\Sigma^+$ SCF MOs as basis for the respective LSC–SO–CI calculations, and these results are compared in Table II. The ground-state total energies at the $\Lambda - S$ level of treatment are $-83.213\,328$ and $-83.213\,559 \, E_h$, respectively at the FCI level of treatment, a difference of only $51 \, cm^{-1}$, indicating a high level of convergence in the corresponding MRD-CI treatments. Moreover, computed transition energies for corresponding levels differ by no more than $600 \, cm^{-1}$, and on the average by less than $230 \, cm^{-1}$.

There is a large splitting for the $X \, ^2\Pi$ state because of the fact that the open-shell MO in the dominant configuration is localized on the lead atom. Computed spectroscopic constants (T_e, r_e, and ω_e values) are compared with experiment[1] for the lowest three Ω states of PbF in Table III. First of all, it is found that the above splitting in the Direct-SO-CI calculations differs by only $23 \, cm^{-1}$ from the corresponding observed value of $8264 \, cm^{-1}$. The two-step value is still of quite respectable accuracy, however, giving an error of $459 \, cm^{-1}$ or 5.5%. Interestingly enough, however, the opposite situation is found for the computed $A \, ^2\Sigma^+_{1/2} T_e$ values. The simpler calculation gives a result which is only $19 \, cm^{-1}$ in error (LSC–SO–CI) for this quantity, whereas the Direct SO-CI value is in error by $668 \, cm^{-1}$ or 3.0%. In the first case, one can argue that the more flexible SO–CI approach is superior because it is better able to describe differences between the Pb $6p$ 1/2 and 3/2 spinors, which is a

J. Chem. Phys., Vol. 116, No. 2, 8 January 2002

Low-lying states of PbF   611

FIG. 2. (a) Computed LSC–SO–CI potential energy curves for various PbF Ω electronic states ($\Omega = 1/2$—solid lines, 3/2—dashed lines, 5/2—dotted line). (b) Computed Direct SO–CI potential energy curves for various PbF Ω electronic states.

TABLE II. Comparison of calculated LSC–SO–CI vertical excitation energies (cm^{-1}) at $r = 3.95\,a_0$ for two different SCF-MO basis sets ($A\ ^2\Sigma^+$ of PbF and $X\ ^1\Sigma^+$ of PbF$^+$).

Ω state	E ($^2\Sigma^+$ MOs)	E ($^1\Sigma^+$ MOs)	Δ
X_1 1/2(I)	0	0	
X_2 3/2(I)	7832	7785	47
A 1/2(II)	22 820	22 838	-18
1/2(III)	37 194	36 939	255
3/2(II)	39 817	39 653	164
1/2(IV)	45 431	45 405	26
3/2(III)	47 036	46 463	573
1/2(V)	47 444	47 028	416
1/2(VI)	48 123	47 696	427
3/2(IV)	51 002	50 704	298

orbit perturbation matrix element between the $X\ ^2\Pi$ and $A\ ^2\Sigma^+$ 1/2 states is underestimated in the latter computation, and this effect then compensates for the overestimation of the $^2\Sigma^+ - ^2\Pi$ excitation energy at the $\Lambda - S$ level of treatment.

The computed bond lengths in the two SO-CI approaches are quite similar in all three cases (Table III), differing by 0.005 Å in the worst case. The calculations overestimate these quantities by 0.01–0.03 Å relative to experiment.[1] The agreement between corresponding computed vibrational frequencies is similar on a percentage basis for the two SO-CI treatments. A slight exception occurs for the $A\ ^2\Sigma^+_{1/2}$ state (16 cm^{-1} discrepancy), probably because the corresponding potential well characteristics are relatively sensitive to the description of large-r interactions, unlike the case for the $X\ ^2\Pi$ pair of Ω states.

One of the advantages of the LSC–SO–CI approach is that it provides a ready analysis of the spin-perturbed wave functions in terms of their respective $\Lambda - S$ component states. The composition of the lowest five Ω states of PbF is given in Table IV for a number of internuclear distances. As expected, the lowest two $\Omega = 1/2$ states are simply mixtures of the $^2\Pi$ and $^2\Sigma^+$ $\Lambda - S$ components. The secondary configuration contributes only 1.5% to the total wave functions in both cases at $r = 3.5\,a_0$. Near the ground-state equilibrium distance at $r = 3.9\,a_0$ this amount increases to 2.7%, by $r = 4.1\,a_0$ it reaches a value of 3.5%, and it continues growing steadily thereafter (7.4% at $r = 4.9\,a_0$). The intermediate 3/2 state is found to be almost pure $X\ ^2\Pi$ throughout the same range of r (Table IV). Finally, the next highest-energy states are composed primarily of the $a\ ^4\Sigma^-$ $\Lambda - S$ state. The 3/2 root has virtually no other important contribution from other states, but the lower-energy 1/2 state has a $3\ ^2\Sigma^+$ component of 8.1% at $r = 3.9\,a_0$.

The computed energy differences of the various atomic limits obtained with large-r molecular calculations are compared with the corresponding experimental values[34] in Table V. In general, the calculations are able to obtain the expected degeneracies for the various dissociating states to a high degree of accuracy [Figs. 2(a) and 2(b)], which is another good indication that the level of treatment is very close to that of a full valence CI. The F($^2P^o$) 3/2–1/2 splitting is computed to be 369 cm^{-1}, as compared to the measured value of 400 cm^{-1}. There are six molecular states which converge to the

critical factor in this computation, than does the two-step approach, which relies on a rather truncated basis of $\Lambda - S$ eigenfunctions to achieve the desired level of accuracy. In the $A\ ^2\Sigma^+$ case there seems to be a cancellation of errors working in favor of the LSC–SO–CI approach. The spin-

TABLE III. Spectroscopic constants (excitation energy T_e, bond length r_e and vibrational frequency ω_e) for various states of the PbF molecule.

State	T_e/cm^{-1}			$r_e/\text{Å}$			ω_e/cm^{-1}		
	LSC–SO–CI	D–SO–CI	Expt.	LSC–SO–CI	D–SO–CI	Expt.	LSC–SO–CI	D–SO–CI	Expt.
$X_1\,^2\Pi_{1/2}$	0	0	0	2.084	2.084	2.058[a]	530	522	507[a]
$X_2\,^2\Pi_{3/2}$	7805	8241	8264[b]	2.066	2.065	2.034[a]	542	537	533[c]
$A\,^2\Sigma^+_{1/2}$	22538	23225	22557[b]	2.168	2.173	2.160[a]	430	414	395[b]

[a]Reference 31.
[b]Reference 32.
[c]Reference 33.

next highest asymptote, $Pb(^3P_1)+F(^2P^o_{3/2})$. Their average computed atomic excitation energy is 7069 cm^{-1}, which underestimates the measured value by 750 cm^{-1}, an error of 9.6%. The next limit again involves the $F(^2P^o_{1/2})$ excited state. In this case, the computed energy difference relative to its 3/2 counterpart is 379 cm^{-1}, slightly closer to the measured value for this quantity already mentioned.

IV. RADIATIVE LIFETIME CALCULATIONS

A. Transition and dipole moments

Fink and co-workers[1] have measured radiative lifetimes of the A and X_2 states of all four stable lead monohalides. The $A\,^2\Sigma^+-X\,^2\Pi$ is the key transition at the $\Lambda-S$ level of treatment and its transition dipole moment value is shown as a function of r in Fig. 3. One can see that it varies strongly with bond distance and that it vanishes at ca. 3.95 a_0, which is close to the equilibrium distance of both the A and X states. For the calculation of spin-forbidden intensities dipole moments of individual $\Lambda-S$ states are often important as well (Fig. 4). For example, the difference in the A and X values makes a significant contribution to the $A-X_1$ μ_z component. It is evident from the above diagram that both states are ion-pair in nature. The $A\,^2\Sigma^+$ dipole moment is every-

where smaller than that of $X\,^2\Pi$, whereby the polarity for both is clearly Pb^+-F^-. The reason for this distinction is the fact that the π^* MO is almost perfectly localized on the lead atom while the σ^* has its center of charge still farther from the F atom. Thus a $\pi^*\rightarrow\sigma^*$ transition tends to move electronic charge in the direction of lead, and thereby lower the value of the dipole moment by roughly 0.27 ea_0 at each bond distance.

At large r, both the A and X (diabatic) potentials cross with repulsive curves dissociating to the neutral ground-state atoms (Fig. 1). As a result, the corresponding dipole moment curves abruptly change shape and fall off to zero values. The same holds true for the $A-X$ transition moment. The Ω-state transition moments are shown in Fig. 5. It is clear that the $A-X_1$ and $A-X_2$ values are very similar to the $\Lambda-S\,^2\Sigma^+-^2\Pi$ results in Fig. 3. The $A-X_2$ (perpendicular) transition moment crosses that of $A-X_1$ near $r=3.6\,a_0$, but the two results never differ by more than a few hundredths of an ea_0. The z component of the $A-X_1$ moment actually decreases at first with increasing r (Fig. 5), contrary to what one would conclude on the basis of simple two-term spin-orbit mixed states. Other contributions control the overall shape of the curve, so that a minimum is reached near $r=4.1\,a_0$. The corresponding X_2-X_1 fine-structure transition

TABLE IV. Percentage composition of the lowest-energy Ω states of PbF at various internuclear distances r.

Ω state	r/a_0	$^2\Pi$	$1\,^2\Sigma^+$	$2\,^2\Sigma^+$	$3\,^2\Sigma^+$	$^2\Sigma^-$	$^4\Sigma^-(3/2)$	$^4\Sigma^-(1/2)$	$2\,^4\Pi$
X_1	3.5	97.4	1.5						
	3.9	96.0	2.7						
	4.5	93.6	5.4						
	4.9	91.6	7.4						
X_2	3.5	98.6							
	3.9	98.8							
	4.5	98.8							
	4.9	98.4							
A	3.5	1.6	96.4						
	3.9	2.9	95.2						
	4.5	5.6	92.1						
	4.9	7.6	89.1						
1/2(III)	3.5			1.0	6.7			88.4	
	3.9				8.7			80.3	
	4.1				9.6	1.9		75.3	5.1
	4.5				5.0	6.0		52.2	
3/2(II)	3.5						98.2		
	3.9						96.5		
	4.1						95.3		

TABLE V. Comparison of calculated and experimental atomic energy limits.

Atomic limit	Ω states	ΔE (Calc.)/cm^{-1}	ΔE^a (Expt.)/cm^{-1}
Pb($^3P_0$)+F($^2P^o_{3/2}$)	1/2, 3/2	0	0
Pb($^3P_0$)+F($^2P^o_{1/2}$)	1/2	369	400
Pb($^3P_1$)+F($^2P^o_{3/2}$)	5/2, 3/2, 3/2, 1/2, 1/2, 1/2	7069	7819
Pb($^3P_1$)+F($^2P^o_{1/2}$)	3/2, 1/2, 1/2	7448	8219

[a]Reference 34.

moment is of similar magnitude at the ground-state equilibrium distance, but it gradually decreases to a zero value at $r=5.2\,a_0$. Again all dipole moment values (Fig. 6) vanish at large r because each of these states goes to neutral atomic limits. The corresponding transition moment values also vanish at large r after the aforementioned crossing of diabatic potentials has occurred.

B. Radiative lifetimes

There are three transition moments involved in the computation of the radiative lifetime of the A state of PbF (Fig. 5). Two of these ($A-X_1$ and $A-X_2$) stem from the allowed $^2\Sigma^+$-$^2\Pi\ \Lambda-S$ transition with perpendicular polarization, while the third is the parallel (z) component for the $A-X_1$ transition. The partial lifetimes computed in the present study for the lowest vibrational levels of the A and X_2 states are given in Table VI. They show that, at least for $v'=0-5$, the dominant contribution to the A state total radiative lifetime does not come from the allowed $A-X\ \Lambda-S$ transition moment but rather from the $A-X_1$ parallel component.

The reason for this, as already indicated in Sec. IV A, is that the Σ^+-Π moment vanishes in the neighborhood of the A state's potential minimum and thus has relatively little influence on the overall emission intensity from this upper state. For $v'=0$, the total lifetime is computed to be 16.1 μs, whereas the parallel component of the $A-X_1$ transition moment corresponds to a partial lifetime which is only 50% longer. By contrast, that for the $A-X_1$ perpendicular transition is nearly 150 μs. The corresponding $A-X_2$ value is about twice as short, but it is still more than four times longer than the total. The latter quantity does not vary at all strongly with v', but the perpendicular $A-X_1$ partial lifetime quickly decreases to the point that it becomes nearly equal to the parallel value at $v'=5$ (Table VI).

The PbF A state's radiative lifetime for $v'=0$ has been measured by Shestakov $et\ al.$[1] to be 5.0$\pm$0.8 μs, which is in quite good agreement with other reported values of Chen $et\ al.$ (4.9$\pm$0.3 μs)[35] and Shestakov $et\ al.$ (5.0$\pm$0.3 μs).[36] The present computed value is thus about three times larger than observed. As Table VI shows, however, the value of the
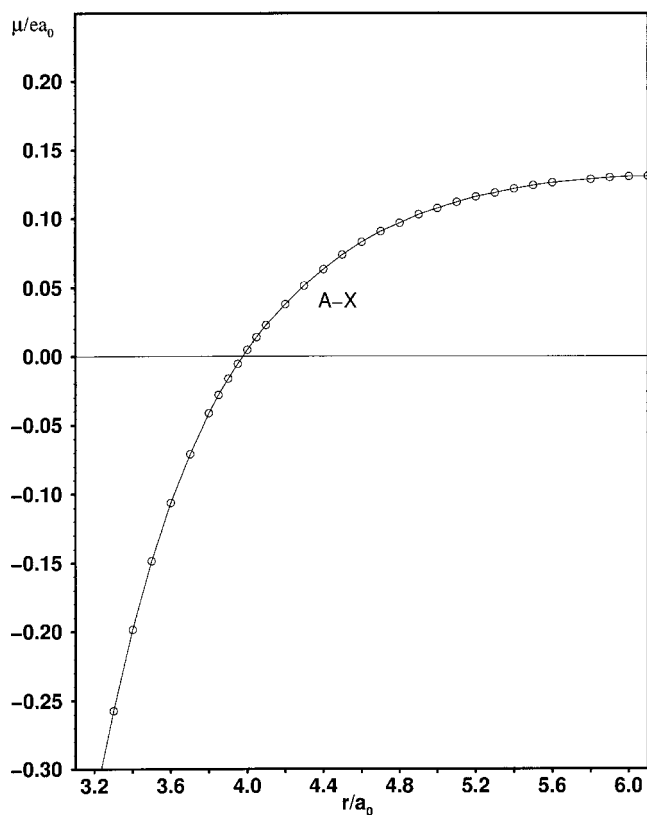

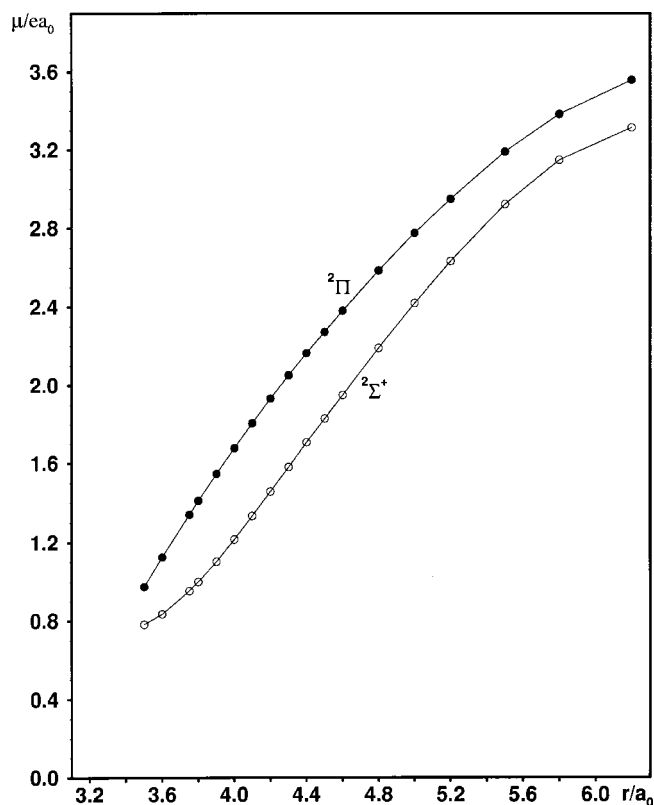FIG. 3. Computed MRD-CI $A-X$ electric dipole transition moment for PbF as a function of internuclear distance r.

FIG. 4. Computed MRD-CI dipole moments for the $X\ ^2\Pi$ and $A\ ^2\Sigma^+$ electronic states of PbF as a function of internuclear distance r obtained without spin-orbit coupling.
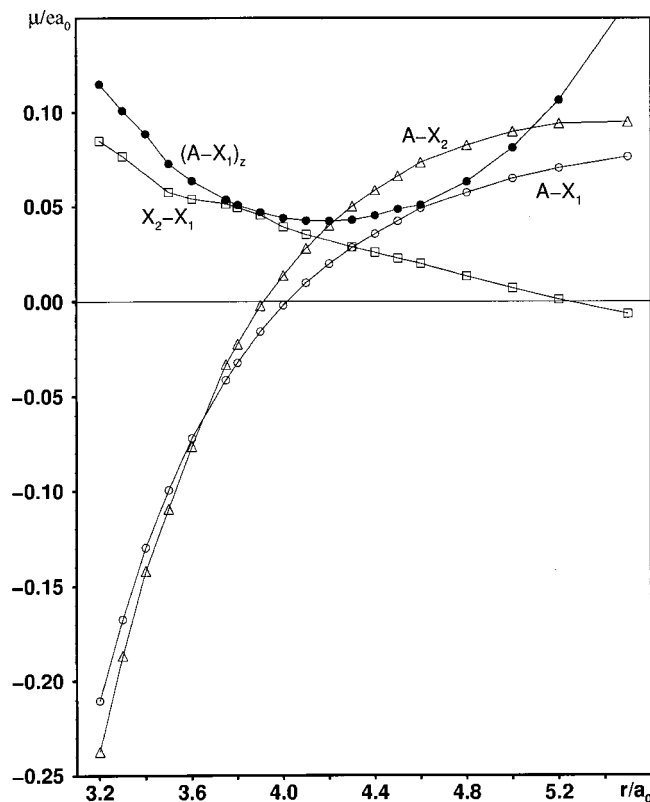
FIG. 5. Computed LSC–SO–CI electric dipole transition moments for various low-lying Ω states of the PbF molecule as a function of internuclear distance r.

FIG. 6. Computed LSC–SO–CI dipole moments for the X_1, X_2 and A electronic states of the PbF molecule as a function of internuclear distance r.

radiative lifetime decreases rather quickly with v', so that it is 9.2 μs at $v' = 5$. This relatively strong dependence on v' is clearly due to the strong variation in the key $A-X$ $\Lambda-S$ perpendicular transition moment (Fig. 3). Probably the simplest way to explain the discrepancy between calculation and experiment for the $v' = 0$ lifetime is to assume that the r value at which the latter transition moment vanishes is as much as 0.03 Å (see Table III) farther removed from the location of the actual potential minimum for the A state than has been found in the present calculations. This eventuality would lead to a significant decrease in the $v' = 0$ partial lifetime for the perpendicular $A-X_1$ transition and thus to a corresponding reduction in its total radiative lifetime, bringing it in far better agreement with the observed value. The z component for the $A-X_1$ transition moment is also fairly sensitive to theoretical treatment because it results from at least three rather small $\Lambda-S$ contributions which are nearly equal in magnitude. In any event, it would be very useful if the A state's radiative lifetime could be measured for more than just the $v' = 0$ level. It is clear from the shape of the computed $A-X$ transition moment (Fig. 3) that this quantity should depend rather strongly on v', and it would be highly desirable to check this result experimentally.

The X_2 radiative lifetime has also been measured,[1,33] and a value of 0.36±0.05 ms has been found, some 72 times longer than for the A state's value. The present computed lifetime values are also given in Table VI as a function of v'. They again show a fairly large discrepancy relative to the observed $v' = 0$ lifetime, but also that the computed lifetime
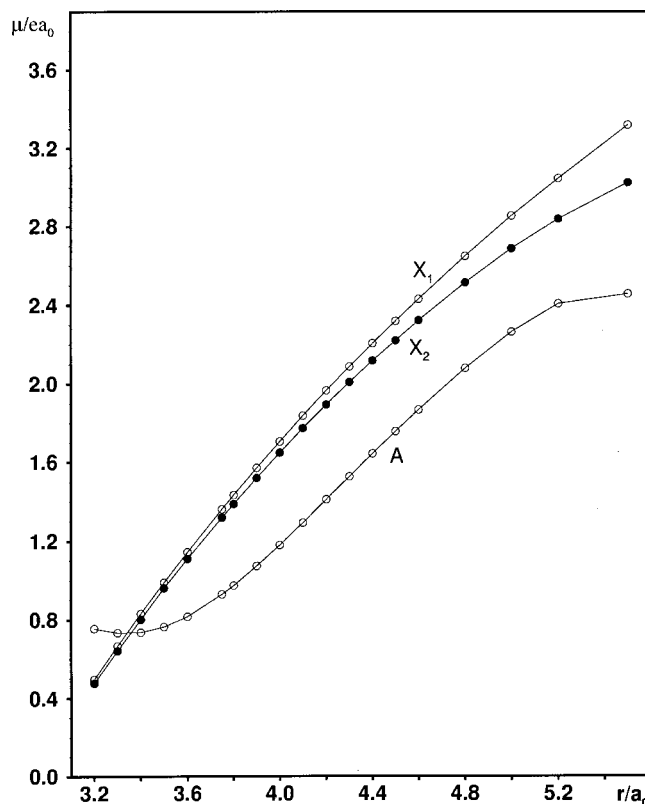
drops rather quickly with v'. For example, for $v' = 3$ the computed X_2 radiative lifetime is 0.39 ms, which is in much better agreement with what has been measured, albeit for $v' = 0$. One should note in general that it is increasingly more difficult to obtain high-percentage accuracy for such quantities as their values increase to the ms range. Thus, the level of agreement found between the present SO–CI calculations and experiment is still quite acceptable for both PbF upper states, and this experience bodes well for the hoped-for goal in the broader study of being able to satisfactorily explain the observed trends in such quantities throughout the lead monohalide series.

TABLE VI. Computed partial and total radiative lifetimes (μs) of the A and X_2 states of PbF for various vibrational levels v'.

v'	$A-X_1(\perp)$	$A-X_1(\parallel)$	$A-X_2(\perp)$	A (total)	X_2 (total)
0	148.6	24.7	67.2	16.1	3374
1	68.1	24.0	64.4	13.9	965
2	44.6	23.3	62.5	12.3	560
3	33.3	22.6	61.9	11.1	395
4	26.6	21.9	61.7	10.1	304
5	22.2	21.3	61.6	9.2	297
6	19.2	20.8	61.6	8.6	209
7	17.0	20.2	61.8	8.0	182
8	15.4	19.5	62.3	7.6	161
9	14.2	18.8	62.8	7.2	144
10	13.2	18.1	63.5	6.8	131
11	12.3	17.4	64.2	6.5	120

V. CONCLUSION

Two different methods for obtaining SO–CI wave functions and energies have been compared in the present study. It was found that the potential curves for the ground and low-lying states of the PbF molecule are quite similar in both approaches and that the results are in good agreement with experiment. This experience demonstrates that the relatively simple method for including spin-orbit effects which has been in use in our laboratory for nearly a decade, namely to form a matrix representation of the full relativistic Hamiltonian in the basis of a small number of $\Lambda - S$ states and then to diagonalize to obtain spin-mixed eigenfunctions and their energy eigenvalues, is quite accurate even for relatively heavy atoms such as lead and bismuth. On the other hand, it is important to have SO–CI programs which are able to work directly with many-electron configuration-state basis functions (or alternatively with Slater determinants) in order to provide checks on the accuracy of the simpler (LSC–SO–CI) method in any given situation, and that goal has been reached in the present study.

It has also been demonstrated that the full-valence CI limit has been closely approximated in the present nine-active-electron multireference treatment. The Ω-state eigenvalues obtained with SCF MOs for both the PbF $^2\Sigma^+$ and the PbF$^+$ $^1\Sigma^+$ states for the first ten roots of the LSC–SO–CI secular equations agree to within an average of less than 230 cm^{-1}. This result also indicates that the core electrons in the CI (Pb $5d$ and F $2s$ shells) are nearly equally well described in these two SCF treatments.

The calculations show that there are only three low-lying Ω states of PbF which are clearly bound, as all other potential curves obtained are either repulsive or have at most weak shoulders. The dominant $\Lambda - S$ excitation is the perpendicular $^2\Sigma^+ - ^2\Pi$ transition, and its dipole moment matrix element is found to depend quite strongly on internuclear distance. It becomes zero in the neighborhood of the A $^2\Sigma^+_{1/2}$ potential minimum, and as a consequence the $A - X_1$ Einstein coefficient of spontaneous emission for the $v' = 0$ upper state is determined primarily from the parallel (z) component of the corresponding transition moment. The corresponding radiative lifetime is calculated to be 16 μs, as compared to the measured value of only 5.0 μs. The analogous results for higher A-state levels decrease rather strongly with v', however, so that a value of 8.6 μs is found for $v' = 6$. It is speculated that a slight shift in the $A - X$ $\Lambda - S$ transition moment curve which would move the aforementioned zero value away from the A-state's Franck–Condon region by as little as 0.03 Å would alter the calculations sufficiently to bring the computed $v' = 0$ radiative lifetime into much better agreement with the measured value. At the same time, one should realize that for such relatively weak transitions, a factor of 2–3 accuracy is not unexpected, so the present discrepancy in the A, $v' = 0$ lifetime can still be considered as acceptably small.

The X_2 radiative lifetime is measured to be 0.36 ms, 72 times longer still than that of the A state. The calculations again find the $v' = 0$ lifetime to be too long compared to this value, but also that the lifetimes of the higher-lying levels gradually decrease with v', so that a value of 0.39 ms is found for $v' = 3$. This result again indicates that a slight shift in the X_1 and X_2 potentials or the corresponding transition moment as a function of internuclear distance would result in notably better agreement between the calculated and actual lifetimes of the vibrational levels of this upper state. Finally, the results of the present calculations appear to be of sufficient accuracy to enable a clear understanding of trends in the A and X_2 radiative lifetimes which have been observed in the lead monohalide series of radicals, and work is in progress to achieve this objective.

[1] O. Shestakov, H. Demes, and E. H. Fink, Chem. Phys. **178**, 561 (1993).
[2] A. B. Alekseyev, H.-P. Liebermann, I. Boustani, G. Hirsch, and R. J. Buenker, Chem. Phys. **173**, 333 (1993).
[3] H.-P. Liebermann, I. Boustani, S. N. Rai, A. B. Alekseyev, G. Hirsch, and R. J. Buenker, Chem. Phys. Lett. **214**, 381 (1993).
[4] K. K. Das, A. B. Alekseyev, H.-P. Liebermann, G. Hirsch, and R. J. Buenker, Chem. Phys. **196**, 395 (1995).
[5] A. B. Alekseyev, K. K. Das, H.-P. Liebermann, R. J. Buenker, and G. Hirsch, Chem. Phys. **198**, 333 (1995).
[6] A. B. Alekseyev, R. J. Buenker, H.-P. Liebermann, and G. Hirsch, J. Chem. Phys. **100**, 2989 (1994).
[7] A. B. Alekseyev, H.-P. Liebermann, G. Hirsch, and R. J. Buenker, J. Chem. Phys. **108**, 2028 (1998).
[8] A. B. Alekseyev, H.-P. Liebermann, R. M. Lingott, O. Bludský, and R. J. Buenker, J. Chem. Phys. **108**, 7695 (1998).
[9] A. B. Alekseyev, H.-P. Liebermann, R. J. Buenker, G. Hirsch, and Y. Li, J. Chem. Phys. **100**, 8956 (1994).
[10] A. B. Alekseyev, H.-P. Liebermann, R. J. Buenker, and G. Hirsch, J. Chem. Phys. **102**, 2539 (1995).
[11] A. B. Alekseyev, A. B. Sannigrahi, H.-P. Liebermann, R. J. Buenker, and G. Hirsch, J. Chem. Phys. **103**, 234 (1995).
[12] K. D. Setzer, E. H. Fink, A. B. Alekseyev, H.-P. Liebermann, and R. J. Buenker, J. Mol. Spectrosc. **206**, 181 (2001).
[13] V. Rai, H.-P. Liebermann, A. B. Alekseyev, and R. J. Buenker, J. Chem. Phys. **114**, 8386 (2001).
[14] K. D. Setzer, C. Uibel, W. Zyrnicki, A. M. Pravilov, E. H. Fink, H.-P. Liebermann, A. B. Alekseyev, and R. J. Buenker, J. Mol. Spectrosc. **204**, 163 (2001).
[15] A. V. Titov, N. S. Mosyagin, A. B. Alekseyev, and R. J. Buenker, Int. J. Quantum Chem. **81**, 409 (2001).
[16] A. B. Alekseyev, K. K. Das, H.-P. Liebermann, and R. J. Buenker (unpublished).
[17] H.-P. Liebermann, A. B. Alekseyev, and R. J. Buenker, LSC–SO–CI and Direct SO–CI Computer Programs of the University of Wuppertal.
[18] S. A. Wildman, G. A. DiLabio, and P. A. Christiansen, J. Chem. Phys. **107**, 9975 (1997).
[19] L. F. Pacios and P. A. Christiansen, J. Chem. Phys. **82**, 2664 (1985).
[20] R. J. Buenker and S. D. Peyerimhoff, Theor. Chim. Acta **35**, 33 (1974).
[21] R. J. Buenker and S. D. Peyerimhoff, Theor. Chim. Acta **39**, 217 (1975).
[22] R. J. Buenker, in *Proceedings of the Workshop on Quantum Chemistry and Molecular Physics*, edited by P. G. Burton (University of Wollongong Press, Wollongong, Australia, 1980).
[23] R. J. Buenker, in *Current Aspects of Quantum Chemistry 1981*, Studies in Physical and Theoretical Chemistry Vol. 21, edited by R. Carbó (Elsevier, Amsterdam, 1982), pp. 17–34.

[24] R. J. Buenker and R. A. Phillips, J. Mol. Struct.: THEOCHEM **123**, 291 (1985).

[25] S. Krebs and R. J. Buenker, J. Chem. Phys. **103**, 5613 (1995).

[26] R. J. Buenker and S. Krebs, in *Recent Advances in Multireference Methods*, edited by K. Hirao (World Scientific, Singapore, 1999), pp. 1–29.

[27] E. R. Davidson, in *The World of Quantum Chemistry*, edited by R. Daudel and B. Pullman (Reidel, Dordrecht, 1974), p. 17.

[28] G. Hirsch, P. J. Bruna, S. D. Peyerimhoff, and R. J. Buenker, Chem. Phys. Lett. **52**, 442 (1977); D. B. Knowles, J. R. Alvarez-Collado, G. Hirsch, and R. J. Buenker, J. Chem. Phys. **92**, 585 (1990).

[29] J. W. Cooley, Math. Comput. **15**, 363 (1961).

[30] M. Perić, R. Runau, J. Römelt, S. D. Peyerimhoff, and R. J. Buenker, J. Mol. Spectrosc. **78**, 309 (1979).

[31] D. J. W. Lumley and R. F. Barrow, J. Phys. B **10**, 1537 (1977).

[32] K. P. Huber and G. Herzberg, *Molecular Spectra and Molecular Structure* (Van Nostrand Reinhold, Princeton, 1979), Vol. 4.

[33] K. Ziebarth, R. Breidohr, O. Shestakov, and E. H. Fink, Chem. Phys. Lett. **190**, 277 (1992).

[34] C. E. Moore, Arch. U.S. Natl. Bur. Stand. **467**, 3 (1971).

[35] J. Chen and P. J. Dagdigian, J. Chem. Phys. **96**, 1030 (1992).

[36] O. Shestakov, A. M. Pravilov, H. Demes, and E. H. Fink, Chem. Phys. **165**, 415 (1992).